Biointerface Research in Applied Chemistry
Open-Access Journal (ISSN: 2069-5837)

Article
Volume 13, Issue 3, 2023, 270
https://doi.org/10.33263/BRIAC133.270

Enhancement Photovoltaic Performance of p-i-n Amorphous Silicon Solar Cells with Intrinsic Layer

Abdellatif Hmairrou [1], El Hadi Chahid [1,2], Mohammed Azza [1], Rachid Abdia [2] Soufiane Belhouideg [2], Malika Tridane [1,3], Abdessamad Malaoui [2], Said Belaaouad [1]

[1] Laboratory of Physical Chemistry of Materials, Faculty of Sciences Ben M'sik, Hassan II University of Casablanca, Morocco
[2] Research Laboratory in Physics and Sciences for Engineers (LRPSI), Polydisciplinary Faculty, Sultane Moulay Slimane University, Beni Mellal, Morocco
[3] Regional Center for Education and Training Occupations, Casablanca Anfa, Bd Bir Anzarane, Casablanca, Morocco
* Correspondence: mohammedazza81@gmail.com (M.A.); abdellatiftisko@gmail.com (A.H.);

Received: 10.05.2022; Accepted: 21.06.2022; Published: 7.07.2022

Abstract: The numerical simulation of a p-i-n amorphous silicon solar cell has been analyzed using the SCAPS-1D software. The effect of the thicknesses of the layers and doping concentration under the standard AM1.5 operating conditions are investigated on the output parameters cell, such as the open-circuit voltage Voc, the short-circuit current density Jsc, the fill factor FF, and the efficiency of power conversion.η. The simulation results indicated that the performance of the studied solar cell is related to temperature, p and n layer doping, and intrinsic layer thickness. The simulations revealed that the cell's performance is affected by these physical and photoelectric parameters. As a result, the experimental data was used to validate the simulation results. The experimental data and the simulation predictions were found to be in good accord. On the other hand, the obtained optimal parameters for high performance offer an efficiency of 11.61% with layer thicknesses (nm) of p, i, and n regions are respectively 9,300,100, and concerning n and p layers doping (cm^{-3}) are respectively 1020 cm^{-3} and 1018 cm^{-3}.

Keywords: photovoltaic cell; J-V characteristic; amorphous silicon; SCAPS-1D; efficiency.

1. Introduction

Energy has been the engine of human activity since antiquity; it plays a very important role in daily life and in the development of nations. Depending on the needs, several forms of energy have appeared as human civilization has developed. Generally, these forms come from fossil energy sources such as coal, oil, natural gas, and uranium [1, 2]. Solar radiations are the most efficient energy source that can be one of the usual alternative energy. To minimize CO_2 emissions from fossil fuels, alternative sources of energy production have been developed with efficiency over the past seven decades using solar energy, which is abundant, clean, free, readily available, and non-toxic and which can be operated in photovoltaic cells that convert sunlight directly into electricity [3, 4]. Different types of solar cell structures have been developed by different technologies, with thin-film technology being the most powerful for large-area production. Amorphous silicon is a material that is increasingly involved in its manufacture because it has the advantage of a relatively low production cost, in addition to being very easy to deposit in thin layers. Still, it is not considered an ideal material for

photovoltaic conversion due to its low absorption of solar radiation, which requires a thick layer to obtain satisfactory results [5-20].

SCAPS (Solar Cell Capacitance Simulator) is a one-dimensional solar cell simulation program developed at the Department of Electronics and Information Systems (ELIS) of Ghent University, Belgium, which is applicable to crystalline and amorphous solar cells such as Si and GaAs family [21]. SCAPS-1D software is used to explore the Silicon amorphous thin-film solar cell in this numerical investigation. It is frequently used to simulate many types of solar cells, and the SCAPS simulation results have been shown to accord well with the corresponding actual data, providing a compelling reason to use it in this study. We've recently used the SCAPS to investigate various thin-film-based solar cells, such as GaAs solar cells [22, 23]. SCAPS uses the Poisson equation along with the hole and electron continuity equations to determine the band diagram in a steady-state, the recombination profile, and carrier transport in one dimension. All of the simulations were carried out in standard conditions of 1000 (W/m^2) light intensity, 300 K temperature, and AM1.5 light spectrum illumination.

In this paper, we present the numerical simulation of amorphous silicon-based on p-i-n junction solar cells to provide guidance for improving performance through device structure modification given available material properties. SCAPS-1D software examined the performance of silicon solar cells by a study of the physical and photoelectrical parameters on the output solar cell characteristic such as the fill factor FF, open-circuit voltage Voc, short-circuit current density Jsc, and conversion efficiency η.

2. Materials and Methods

2.1. p-i-n structure of a-Si solar cell.

The schematic conventional of a p-i-n single-junction solar cell employed in the simulation is shown in Figure 1 [24]. It consists of an absorbent layer which is the p-i-n junction based on amorphous silicon. Whereas the front contact layer is formed by a transparent conductive oxide (TCO) layer, and the back contact consists of a highly reflective metallic layer.

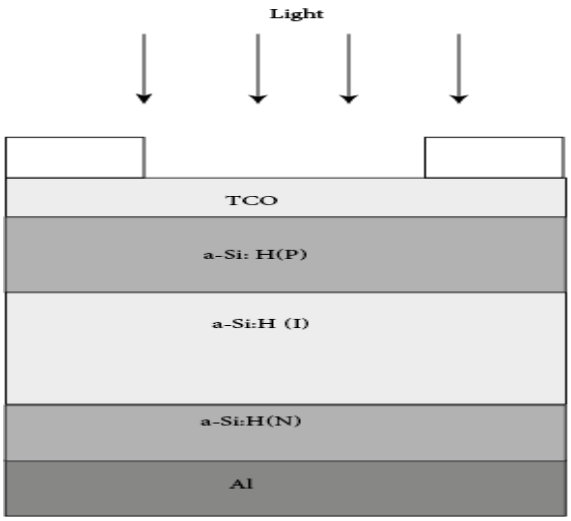

Figure 1. Structure of p-i-n amorphous silicon solar cell**.**

The solar cell parameters employed in this simulation are commonly available and can be found in Table 1 [24].

Table 1. Physical parameters of a-Si:H used in the simulation.

Parameters	p-layer	i-layer	n-layer
Thickness (nm)	9	500	20
ε_r	7.2	11.9	11.9
χ_e(eV)	3.9	3.9	3.9
E_g(eV)	1.8	1.8	1.8
$\mu_n(cm^2.V^{-1}.s^{-1})$	20	20	20
$\mu_p(cm^2.V^{-1}.s^{-1})$	5	5	5
$N_C(cm^{-3})$	10^{20}	10^{20}	10^{20}
$N_V(cm^{-3})$	10^{20}	10^{20}	10^{20}
$N_A(cm^{-3})$	10^{17}	0	0
$N_D(cm^{-3})$	0	0	10^{17}

SCAPS-1D software uses finite difference and Newton-Raphson methods to solve basic semiconductor equations [25]. All simulations were carried out in standard conditions of 1000 (W/m^2), the temperature of 300 K, and the illumination of the AM1.5 light spectrum. The performance parameters of solar cells, such as Voc, Jsc, FF, and conversion efficiency, are explored by including the different material properties in SCAPS-1D. This numerical simulation establishes the solution of the Poisson equation and continuity equations for electrons and holes in a 1-D state and under steady conditions [26]. The Poisson equation is described as follows:

$$\frac{\partial}{\partial x}\left(\varepsilon\frac{\partial\phi}{\partial x}\right) = q[p(x) - n(x) + N_D - N_A] \quad (1)$$

where ϕ, q, and ε are respectively the electrostatic potential, free charge of the electron, and dielectric permittivity of the material. n and p are the free electrons and hole densities. N_A and N_D are donors and acceptors concentrations, respectively.

The semiconductor continuity equations for electrons and holes in the steady-state are given as follows:

$$\frac{\partial J_n}{\partial x} = G_p - R_n \quad (2)$$

$$\frac{\partial J_p}{\partial x} = G_p - R_p \quad (3)$$

The current densities of electrons J_n and holes J_p occur by drift and diffusion process, and can be described using the following equations:

$$J_n = D_n\frac{\partial n}{\partial x} + n\mu_n\frac{\partial\phi}{\partial x} \quad (4)$$

$$J_p = D_p\frac{\partial p}{\partial x} + p\mu_p\frac{\partial\phi}{\partial x} \quad (5)$$

D_n, D_p and μ_n , μ_p are the diffusion coefficients and mobility's electrons and holes, respectively. G_p and R_p describe the creation process and recombination rate of free electron-hole pairs [26].

To have a convergence of solutions, SCAPS uses the boundary conditions at each region cell [27]. At the top contact (x=0):$S_n\Delta n = D_n\frac{\partial n}{\partial x}\Big|_{x=0}$, where S_n is the surface recombination velocity, and at junction between p-layer and intrinsic i-layer, the minority carriers' doping concentration has remained constant. It can be calculated using the equation: $(x = x_p), n = n_{p_0} = \frac{n_i^2}{N_a}\Big|_{x=x_p}$

The efficiency η of a solar cell is the most often used criterion for comparing its performance to that of another. The efficiency of a solar cell is defined as the ratio of energy production to energy input from the sun. Particularly, the fraction of incident power P_{in} converted to electricity determines a solar cell's efficiency, which is given by [28]:

$$\eta = \frac{P_{max}}{P_{in}} = \frac{V_{oc}\, I_{sc}\, FF}{P_{in}} \quad (6)$$

where V_{oc} is the open-circuit voltage, I_{sc} is the short circuit current, and FF is the fill factor. The input power P_{in} for efficiency, calculation is $100\ mW/cm^2$.

3. Results and Discussion

The performance of amorphous silicon solar cells based on p-i-n single-junction was investigated in this study. After simulating the cell structure using SCAPS-1D, the obtained power conversion efficiency for an a-Si solar cell with short circuit current density Jsc, open-circuit voltage Voc, fill factor FF, and efficiency η are listed in Table 2, and the characteristics both of our numerical simulation results and experimental values [29] are represented in Figure 2.

Table 2. Comparison between Simulated and experimental values of an a-Si:H solar cell.

Junction type	$V_{co}(V)$	$J_{sc}(mA/cm^2)$	$FF(\%)$	$\eta(\%)$
Simulation values	0.96	17.39	69.10	11.53
Experimental values [15]	0.82	16.79	68.2	9.51

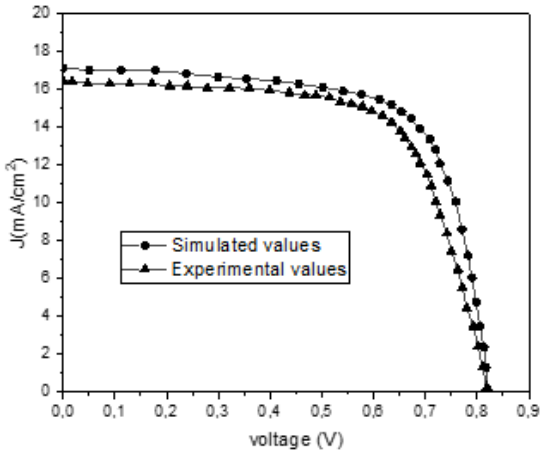

Figure 2. Experimental and simulated values of p-i-n a-Si:H.

To validate our simulation results, we compare the density current-voltage (J-V) characteristic related to the experimental and simulation data. Figure 2 presents the results of the experimental values and our simulation results obtained by the SCAPS-1D software.It is noted that the simulation values are comparable to the experimental values, demonstrating the accuracy of our findings. On the other hand, It is noted that the use of the intrinsic layer' i' in the p/n- junction has increased the short circuit current density J_{sc}, the fill factor and the conversion efficiency. The power conversion efficiency is estimated at 11.61 % for using the amorphous silicon.

3.1. Effect of intrinsic layer thickness.

We'll investigate to study the variations of the characteristics of the cell according to the thickness of the intrinsic layer i because this layer plays a very important role in the

photovoltaic properties of the cell, especially during the absorption phenomena. Figure 3 shows a summary of the obtained results. The inclusion of the intrinsic layer' i' causes an increase in cell efficiency, demonstrating the relevance of this layer in thin-film solar cells based on a-Si:H.

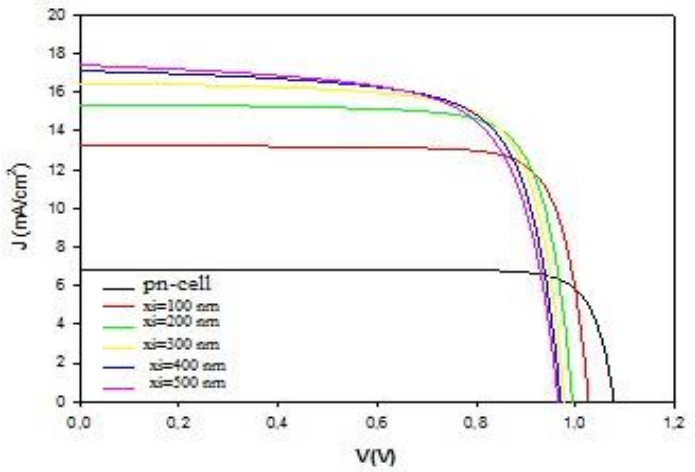

Figure 3. Effect of the thickness of the i- layer on the J-V characteristic.

Figure 4 shows the effect of the intrinsic layer thickness on the output J-V characteristic of the cell. We note that an increase in the intrinsic layer improves the short-circuit current, decreases the open-circuit voltage, and consequently improves the energy conversion efficiency. Furthermore, when the thickness of the i-layer is raised from 100 nm to 500 nm, Voc and FF decrease while Jsc increases. For an i-layer thickness of 300 nm, the cell's power conversion efficiency reaches an optimum of 12.03 %.

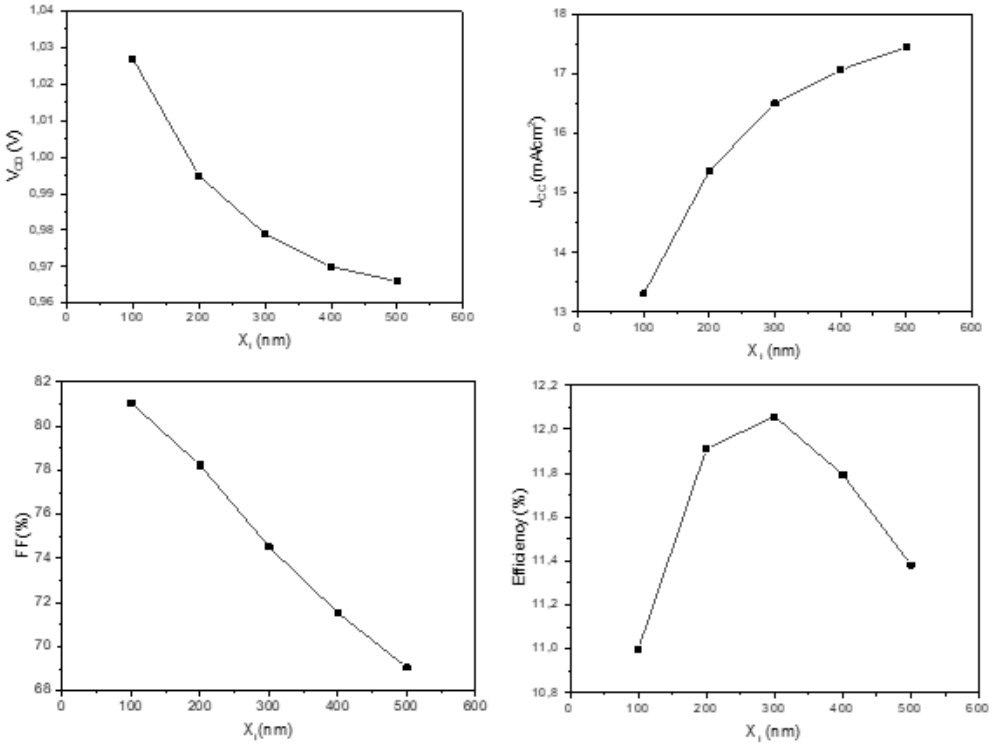

Figure 4. Influence of i-layer thickness on Voc, JSC, FF, and η.

Figure 5 shows the quantum efficiency (QE) of the p-i-n solar cell as a function of the wavelength (nm) of solar radiation. It can be observed that the absence of the i-layer shows a low absorption of photons which causes a decrease in the quantum efficiency QE. It is noted

that there is a significant decrease in the quantum efficiency QE for wavelengths below 500 nm and an increase for wavelengths above 500 nm. As a result, the intrinsic layer plays a very important role in the thin-film solar cell, especially during absorption phenomena

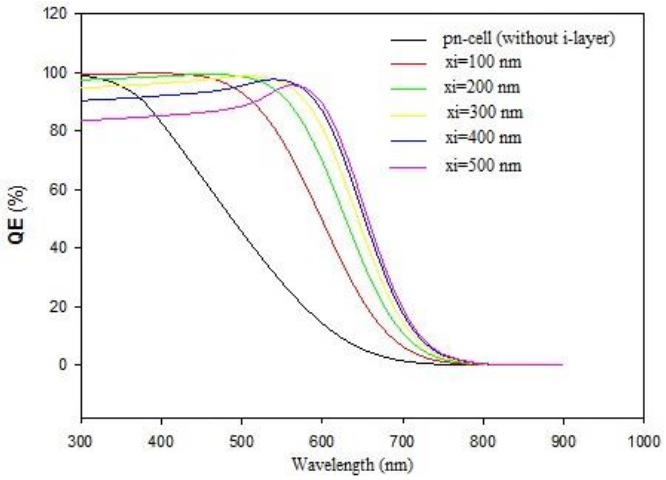

Figure 5. Effect of intrinsic layer thickness on the quantum efficiency (QE).

3.2. Effect of p layer thickness.

Figure 6 shows the effect of the P layer thickness on open-circuit voltage Voc, short circuit current Jsc density, fill factor FF and power conversion efficiency η.

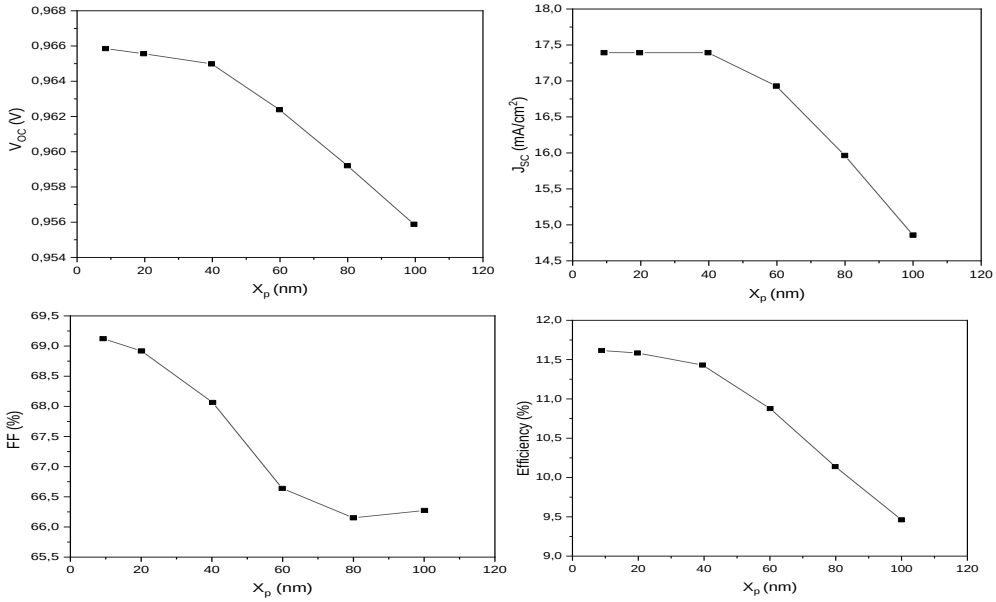

Figure 6. Effect of p layer thickness on the V_{oc}, J_{sc}, FF, and η.

It can be seen that the open-circuit voltage, fill factor, and efficiency is maximum at 9 nm and then decrease as the p layer thickness increases. However, the short-circuit current density is stable up to 40 nm and then varies in an inverse manner. From this simulation, we can conclude that the optimum thickness for the p layer is 9 nm and corresponds to maximum efficiency of 11.61 %.

3.3. Effect of Na doping.

We study the influence of doping N_a of the p layer on the J-V characteristic and subsequently on the performance of the cell.

Figure 7 shows the effect of doping on the short circuit current density J_{sc}, open-circuit voltage V_{oc}, fill factor FF, and finally on the efficiency η. These parameters are all affected by the variation of the p layer doping N_a. On the one hand, they rise as the doping Na rises from 10^{16} cm^{-3} to 10^{18} cm^{-3}, and then they remain nearly constant over the whole doping range from 10^{19} cm^{-3} to 10^{20} cm^{-3}. On the other hand, the current density J_{sc} increases with increasing doping until it reaches a maximum of 10^{18} cm^{-3} and then starts to decrease slightly. We conclude that These observations confirm that the doping Na has an optimal value of 10^{18} cm^{-3}, which produces an optimal power conversion efficiency of 11.69 %.

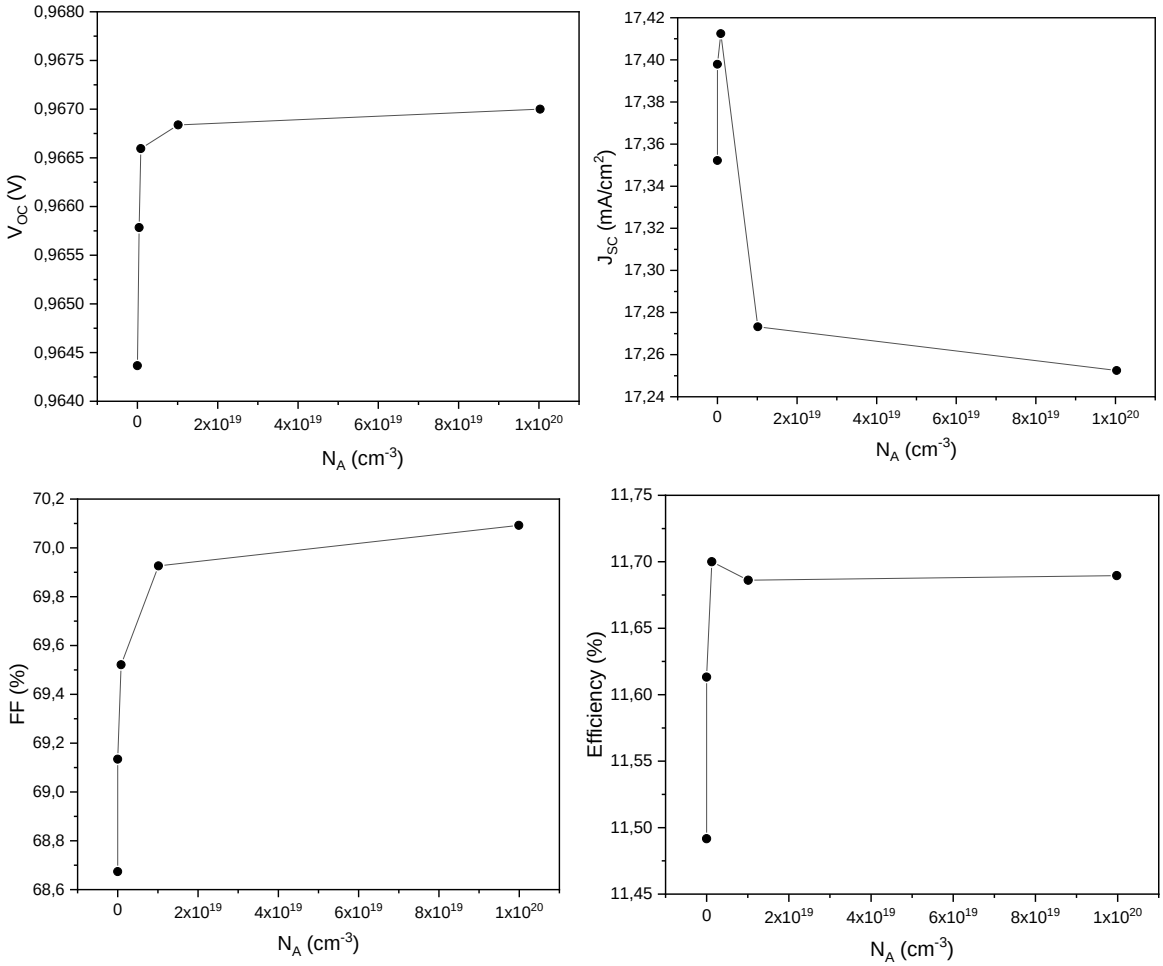

Figure 7. Doping effect of the p-layer on V_{oc}, J_{sc}, FF, and η**.**

3.4. Geometrical and physical parameters of n layer effect.

We are interested in the influence of the physical and geometrical proprieties of n-layer, in particular, its thickness x_n and doping N_d.

3.4.1. Effect of n- layer thickness x_n.

In the following figure, the simulation results of the output photoelectrical parameters V_{oc}, J_{sc}, FF, and η are displayed with a variation of the n- layer thickness.

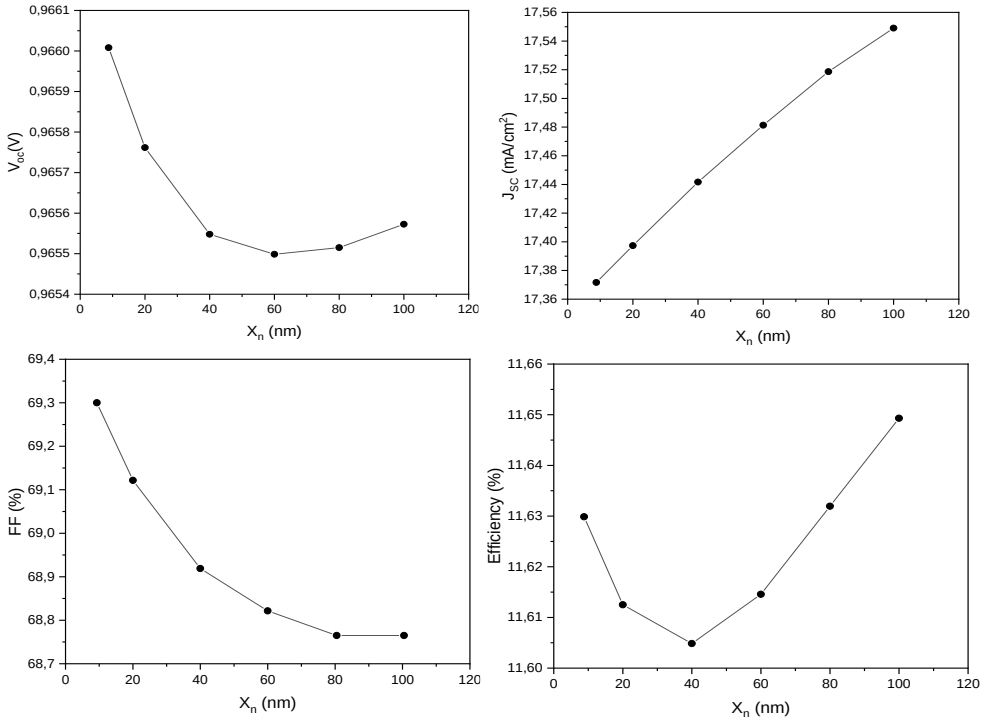

Figure 8. Effect of n- layer thickness on V_{oc}, J_{sc}, FF, and η.

We can observe that as the n-layer thickness increases, the short-circuit current density increases while the open-circuit voltage and the fill factor decrease. Besides, the cell efficiency drops until it reaches its lowest point at 40 nm and then begins to rise. It is concluded that the optimum value for the n-layer thickness is 100 nm corresponding to an optimal value of power conversion efficiency.

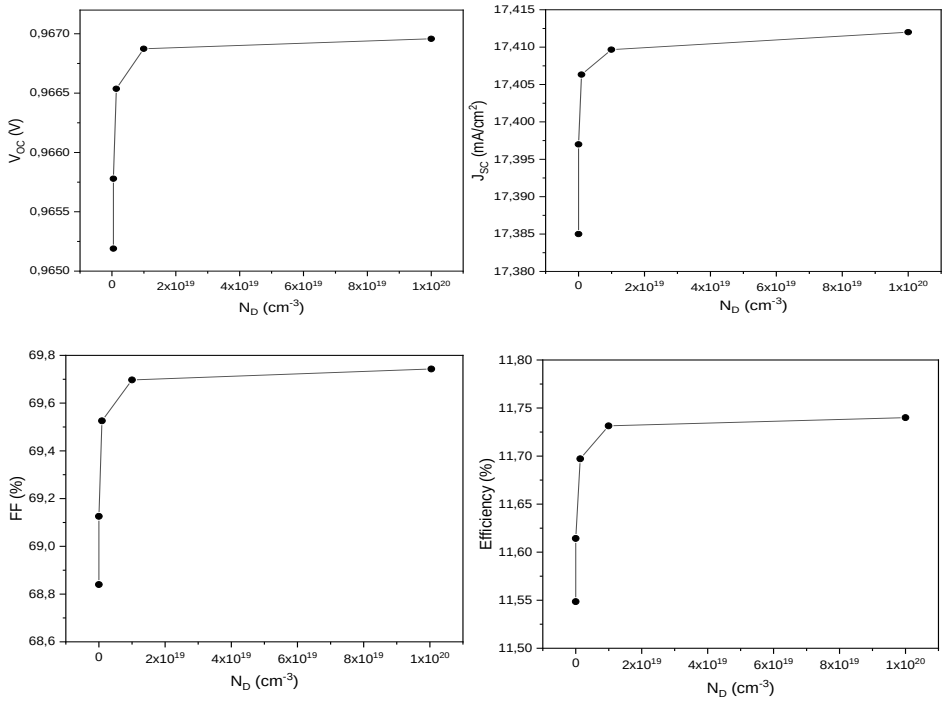

Figure 9. Influence of ND doping on photovoltaic parameters.

3.4.2. Effect of N_D doping.

The effect of doping N_D on short circuit current density J_{sc}, open-circuit voltage V_{oc}, fill factor FF, and efficiency η is shown in Figure 9. We can observe that the n-layer doping

N_D has an effect on these parameters; in particular, they rise as the doping level increases. The optimal doping value is discovered to be $N_D = 10^{20} cm^{-3}$, which gives a maximum energy conversion efficiency.

A comparison of the simulated and experimental p-i-n solar cells is presented in Table 3. It can be summarized that there is an acceptable agreement between the experimental and simulated values.

Table 3. Experimental and simulation results.

Parameters	Experimental	Simulation
V_{oc}(V)	0.82	0.96
J_{sc}(mA/cm^2)	18.3	17.39
FF(%)	68.3	69.11
η(%)	10.3	11.61

4. Conclusions

We have studied the numerical simulation of the p-i-n amorphous silicon solar cell using the SCAPS software. The influence of the intrinsic layer on the operation of the studied cell is investigated. Besides, we have studied the physical and geometrical parameters such as p- and n-layer doping and their thicknesses. The simulation results indicate that the behavior of the p-i-n solar cell is closely related to these parameters. Indeed, after simulating the a-Si:H cell structure using SCAPS-1D, the obtained power conversion efficiency of 11.61% with thicknesses (nm) of p, i, n regions are respectively 9,300,100 , and donor doping layer of 10^{20} cm^{-3}, and acceptor doping layer of 10^{18} cm^{-3}.

Funding

This research received no external funding.

Acknowledgments

The authors would like to thank Prof. Dr. Marc Burgelman, University of Gent, Belgium, for providing the SCAPS simulation software.

Conflicts of Interest

The authors declare that there is no conflict of interests regarding the publication of this paper.

References

1. Oliva, D.; Cuevas, E.; Pajares, G. Parameter identification of solar cells using artificial bee colony optimization. *Energy* **2014**, *72*, 93-102, https://doi.org/10.1016/j.energy.2014.05.011.
2. AlHajri, M.F.; El-Naggar, K.M.; AlRashidi, M.R.; Al-Othman, A.K. Optimal extraction of solar cell parameters using pattern search. *Renewable energy* **2012**, *44*, 238-245, https://doi.org/10.1016/j.renene.2012.01.082.
3. Ishaque, K.; Salam, Z.; Taheri, H.; Shamsudin, A. A critical evaluation of EA computational methods for photovoltaic cell parameter extraction based on twodiode model. *Solar Energy* **2011**, *85*, 1768–1779, https://doi.org/10.1016/j.solener.2011.04.015.
4. Abed, F.A.; Ali, L.M. Investigation the absorption efficiency of GaAs/InAs nanowire solar cells. *Journal of Luminescence* **2021**, *237*, 118171, https://doi.org/10.1016/j.jlumin.2021.118171.
5. Guyomard, D. Mise au Principes de base de l'électrochimie des semi-conducteurs. *Journal de chimie physique* **1986**, *83*, 355-391, https://doi.org/10.1051/jcp/1986830355.

6. Chahid, E.; Feddaoui, M.; Nachaoui, M.; Chowdhury, N.R.; Malaoui, A. Development of Numerical Method for optimizing Silicon Solar Cell Efficiency. *Journal of Nano- And Electronic Physics* **2017**, *9*, 04019, https://doi.org/10.21272/jnep.9%284%29.04019.
7. Azza, M.; Daaif, J.; Chadid, E.H.; Salah, M.; Belaaouad, S. Theoretical Aspect of Physical Phenomena in Inorganic Photovoltaic Cells. Electrical Modeling and Numerical Simulation. *E3S Web of Conferences* **2021**, *297*, 01024, https://doi.org/10.1051/e3sconf/202129701024.
8. Azza, M.; Daaif, J.; Aouidate, A.; Chadid, E.H.; Belaaouad, S. Automatic solution for solar cell photo-current prediction using machine learning. *E3S Web of Conferences* **2021**, *297*, 01029, https://doi.org/10.1051/e3sconf/202129701029.
9. Kerraj, S.; Salah, M.; Chtita, S.; El Idrissi, M.; Belaaouad, S.; Mohammed, M.; Acharjee, N.; Komiha, N. Theoretical study of photovoltaic performances of Ru, Rh and Ir half sandwich complexes containing N, N chelating ligands in Dye-Sensitized Solar Cells (DSSCs). DFT and TD-DFT investigation. *Computational and Theoretical Chemistry* **2022**, *1209*, 113630, https://doi.org/10.1016/j.comptc.2022.113630.
10. Majdi, E.M.; Zerraf, S.; Belhabra, M.; Belaaouad, S. Chemical preparation, crystal structure and vibrational study of $MnNa_3P_3O_{10}$. $12H_2O$ and X-ray characterization of the new anhydrous triphosphate $MnNa_3P_3O_{10}$. *Phase Transitions* **2022**, *95*, 50-63, https://doi.org/10.1080/01411594.2021.2009478.
11. Saouti, F.; Belaaouad, S.; Cherqaoui, A.; Naimi, Y. Polyaniline Thin Film Prepared by Electrochemical Polymerization Method. *Biointerface Research in applied chemistry* **2022**, *12*, 5523 -5533, https://doi.org/10.33263/BRIAC124.55235533.
12. Majdi, E.M.; Belhabra, M.; Ouasri, A.; Fahim, I.; Essehli, R.; Belaaouad, S. Chemical Preparation, Crystal Structure Reinvestigation and Vibrational Study of $CoNa_3P_3O_{10}{\cdot}12H_2O$ and X-ray Characterization of the New Anhydrous Triphosphate $CoNa_3P_3O_{10}$. *Biointerface Research in Applied Chemistry* **2021**, *12*, https://doi.org/10.33263/briac122.25862602.
13. Bassam, R.; El Hallaoui, A.; El Alouani, M.; Jabrane, M.; El Khattabi, E.H.; Tridane, M.; Belaaouad, S. Studies on the Removal of Cadmium Toxic Metal Ions by Natural Clays from Aqueous Solution by Adsorption Process. *Journal of Chemistry* **2021**, *2021*, 7873488, https://doi.org/10.1155/2021/7873488.
14. El Makhloufy, S.; Oubouaza, R.; Ouasri, A.; Belaaouad, S. X-Ray diffraction and infrared spectroscopy data review analyses of the Calcium phosphates. *Biointerface Res. Appl. Chem* **2022**, *12*, 732-755, https://doi.org/10.33263/BRIAC121.732755.
15. Oubouaza, R.; Benson, M.; Wojciechowski, J.; Chtita, S.; Tridane, M.; Belaaouad, S. Synthesis, Crystal Structure, Vibrational Study and DFT Computation of Barium Dihydrogenomonophosphate $Ba(H_2PO_4)_2$. *Biointerface Res. Appl. Chem* **2022**, *12*, 1120-1133, https://doi.org/10.33263/BRIAC121.11201133.
16. El Makhloufy, S.; Belhabra, M.; Zerraf, S.; Ouasri, A.; Chtita, S.; Saadi, M.; El Ammari, L.; Belaaouad, S. Synthesis, Crystal Structure, IR spectroscopy, and DFT computation of the new variety of 2-carboxyanilinium dihydrogen phosphate ($C_7H_8NO_2^+$, $H_2PO_4^-$). *Journal of Molecular Structure* **2021**, *1242*, 130707, https://doi.org/10.1016/j.molstruc.2021.130707.
17. Zerraf, S.; Belhabra, M.; Tridane, M.; Belaaouad, S. Chemical preparation, thermal behavior and IR studies of the New chromium diphosphate hydrate and crystal structure of its corresponding anhydrous. *Biointerface Res. Appl. Chem* **2021**, *11*, 13412-13420, https://doi.org/10.33263/BRIAC115.1341213420.
18. Majdi, E.M.; El Makhloufy, S.; Ouasri, A.; Saadi, M.; El Ammari, L.; Belaaouad, S. Chemical preparation, crystal structure reinvestigation, and vibrational study of meta-carboxyphenyl ammonium dihydrogenomonophosphate $(C_7H_4NH_3OOH)H_2PO_4$(m-CAMP). *Molecular Crystals and Liquid Crystals* **2021**, *714*, 14-25, https://doi.org/10.1080/15421406.2020.1848255.
19. Bassam, R.; El Alouani, M.; Maissara, J.; El Kattabi, L.H.; Rachdi, Y.; Jarmouni, N.; Chbihi, M.E.M.; Belaaouad, S. Physico-chemical characterization of natural rocks and their valorization on the removal of arsenic from aqueous solution. *Materials Today:Proceedings* **2022**, *58*, 1011-1019, https://doi.org/10.1016/j.matpr.2021.12.498.
20. Jarmouni, N.; Tomaiuolo, M.; Gabbani, A.; Genovese, D.; Pineider, F.; Bassam, R.; Belaaouad, S.; Benmokhtar, S. Low temperature synthesis of ultra-green luminescent colloidal $FAPbBr_3$ perovskite nanocrystals. *Materials Today: Proceedings* **2022**, *58*, 1480-1484, https://doi.org/10.1016/j.matpr.2022.02.562.
21. Burgelman, M.; Decock, K.; Khelifi, S.; Abass, A. Advanced electrical simulation of thin film solar cells. *Thin Solid Films* **2013**, *535*, 296-301, https://doi.org/10.1016/j.tsf.2012.10.032.
22. Movla, H. Optimization of the CIGS based thin film solar cells: Numerical simulation and analysis. *Optik* **2014**, *125*, 67-70, https://doi.org/10.1016/j.ijleo.2013.06.034.

23. Burgelman, M.; Verschraegen, J.; Degrave, S.; Nollet, P. Modeling Thin film PV Devices. *Prog. Photovoltaics* **2004**, *12*, 143-153, https://doi.org/10.1002/pip.524.
24. Smucker, J.; Gong, J. A comparative study on the band diagrams and efficiencies of silicon and perovskite solar cells using wxAMPS and AMPS-1D. *Solar Energy* **2021**, *228*, 187-199, https://doi.org/10.1016/j.solener.2021.09.066.
25. Dutta, U.; Chatterjee, P. The open circuit voltage in amorphous silicon *p-i-n* solar cells and its relationship to material, device and dark diode parameters. *Journal of Applied Physics* **2004**, *96*, 2261–2270, https://doi.org/10.1063/1.1769092.
26. Belfar, A.; Aït-Kaci, H. Back reflection and temperature effects on n-i-p-p^+ amorphous and nanocrystalline silicon based solar cells performances. *Optik* **2016**, *127*, 8963–8969, https://doi.org/10.1016/j.ijleo.2016.06.118.
27. Sze, S.M.; Ng, K.K. *Physics of semiconductor devices* **2007,** John Wiley & Sons, Inc., Hoboken, New Jersey, USA.
28. Tiwari, B.; Hossain, M.J.; Bhattacharya, I. GaP/InGaAs/InGaSb triple junction current matched photovoltaic cell with optimized thickness and quantum Efficiency. *Solar Energy* **2016**, *135*, 618–624, https://doi.org/10.1016/j.solener.2016.06.032.
29. Wada, H.; Nishikubo, K.; Sichanugrist, P.; Konagai, M. Improved light trapping effect for thin-film silicon solar cells fabricated on double-textured white glass substrate. *Canadian Journal of physics* **2014**, *92*, 1-4, https://doi.org/10.1139/cjp-2013-0621.